Computationally Guided Tuning of Peptide-Conjugated Perylene Diimide Self-Assembly

Sayak Subhra Panda[†], Kirill Shmilovich[¶], Nicholas S.M. Herringer[¶], Nicolas Marin[†], Andrew L. Ferguson[¶], and John D. Tovar^{†,‡,*}

[†] Department of Chemistry, Johns Hopkins University, 3400 North Charles Street, Baltimore, Maryland 21218, United States.

[‡] Department of Materials Science and Engineering, Johns Hopkins University, 3400 North Charles Street, Baltimore, Maryland 21218, United States.

[¶] Pritzker School of Molecular Engineering, University of Chicago, 5640 South Ellis Avenue, Chicago, Illinois, 60637, United States.

^{*}Corresponding author email: tovar@jhu.edu

Abstract

Peptide- π conjugated materials are important for bio-interfacing charge-transporting applications due to their aqueous compatibility and formation of long-range π -electron networks. Perylene diimides (PDIs), well-established charge-transporting pi-systems, can self-assemble in aqueous solutions when conjugated with amino acids. In this work, we leveraged computational guidance from our previous work to access two different self-assembled architectures from PDI-amino acid conjugates. Furthermore, we expanded the design rule to other sequences to learn that the closest amino acids to the π -core have a significant effect on the photophysical properties of the resulting assemblies. By simply altering glycine to alanine at the closest residue position, we observed significantly different electronic properties as revealed through UV-vis, photoluminescence and circular dichroism spectroscopies. Accompanying molecular dynamics simulation revealed two distinct types of self-assembled architectures: co-facial structures when the smaller glycine residue is at the closest residue position to the π -core versus rotationally-shifted structures when glycine is substituted for the larger alanine. This study illustrates the use of tandem computation and experiment to unearth and understand new design rules for supramolecular materials, and exposes a modest amino acid substitution as a means to predictably modulate the supramolecular organization and engineer the photophysical properties of π -conjugated peptidic materials.

Introduction

Self-assembling π -conjugated materials have emerged as an attractive platform to create functional nanoscale electronic materials from molecular building blocks. ¹⁻⁵ The gradual growth in the field of bionanotechnology encouraged researchers to look into biocompatible π -conjugated materials with electroactive properties. ⁶⁻¹⁰ Due to their ability to form supramolecular architectures through a range of non-covalent interactions, peptides were coupled with π -chromophores to form ordered structures, thus achieving long-range conduction pathways through π -electronic regions in aqueous conditions. ¹¹⁻¹³ The resulting π -conjugated peptide materials can be used to construct field-effect transistors, solar cells or photoconductors based on their ability to transport charges. ¹⁴⁻¹⁷ Incorporation of π -conjugated groups within the peptidic segments introduces quadrupolar interactions that represent substantial perturbations from natural peptide systems. Hence, a delicate balance between non-covalent interactions is necessary to predictably design the optoelectronic outcome of peptide- π conjugates.

Differing electronic interactions that arise from the quadrupolar interactions of π -chromophores in hierarchical suparamolecular structures can lead to different optoelectronic and electrical properties. ^{18, 19} Supramolecular electronic materials are particularly versatile compared to polymeric and single-crystal π -conjugated systems because their macroscopic properties are easily tunable via relatively small changes in the choice of monomeric building blocks. ^{1, 2} Peptides offer a powerful route to such tuning because their side-chains can influence a vast range of properties based on local differences in hydrophobicity, acidity, or polarity; hence, sequence variation is often exploited to achieve a diverse range of peptidic π -electron structures and functions. For example, we previously observed excitonic or excimeric interactions in supramolecular peptide- π conjugated systems that were dictated by the side-chain hydrophobicity

of the constituent amino acids.²⁰ The chirality of individual amino acids (D- or L- configurations) also serves as a point of variation to tune electronic properties at the supramolecular level.²¹⁻²³ Moreover, the positional isomerism of different peptide sequences imparts variation of macroscopic and microscopic properties.²⁴ All of these types of structure variations are readily accessible due to the ease of solid-phase peptide synthesis (SPPS), thus achieving rapid variation of morphological and optoelectronic properties of the self-assembled structures.

Perylene diimides (PDIs) were investigated extensively due to their excellent optoelectronic and electrical properties.²⁵⁻²⁸ The high electron affinity and relatively efficient charge transport properties make PDIs useful n-type materials in different organic electronic devices such as field-effect transistors, 29 solar cells 30 and light-emitting diodes 31. Their macroscopic properties can be tuned easily by variation of the functionalizing group at the imide nitrogen position and on the 'bay' regions of the perylene, which can lead to significant differences in the orientation and separation (both longitudinal and transverse direction) of inter-chromophore packing and subsequently in the observed optoelectronic and electrical properties.³² PDIs were coupled with single amino acids at both ends and their impact on optoelectronic properties was investigated.³³⁻³⁶ For example, Adams and co-workers investigated optoelectronic properties of several peptide-PDI conjugates in solution and gel form by systematically varying the amino acids with aliphatic and aromatic side chains.^{34, 35} Polypeptide-PDI conjugates have been also studied previously.³⁷⁻⁴¹ Hodgkiss and co-workers identified potentially three different states of PDI chromophores within the aggregates: monomeric, H-aggregated and π -aggregated that shows a broad, featureless signal similar to liquid crystalline forms.^{37,38} These broad featureless absorption signals were explained as a mixture of H-type and J-type aggregates by Frauenrath and coworkers.⁴⁰ However, a predictable trend of optoelectronic properties of peptide-PDI conjugates based on the amino acid sequences remains elusive.

Recently, Thurston and Ferguson conducted molecular dynamics simulations of selfassembled peptides with D-X₁-X₂-X₃ sequences conjugated to a PDI core. ⁴² They developed a key metric 'α' which corresponds to the ratio of 'aligned' oligopeptides in a cluster to the 'associated' oligopeptides in a cluster. Two peptides are said to be 'associated' if the distance between any two of their atoms is less than 0.5 nm. Similarly, peptides were designated as 'aligned' if the distance between the atoms in the π -core is less than 0.5 nm. This metric provides a way to quantify the good geometric alignment of the π -cores within the oligopeptide self-assembly. New peptides DAVG-PDI-GVAD ($\alpha = 0.64 \pm 0.07$) and DAIA-PDI-AIAD ($\alpha = 0.58 \pm 0.05$) were identified to have high cofacial intermolecular alignment, but until now had not been synthesized and characterized experimentally. In this report, we describe the optoelectronic properties of these two peptides, showing two very different outcomes within self-assembled nanomaterials derived from them. To further challenge this finding, we report here a small library of PDI-peptide conjugates that vary by the nature of the amino acid residues closest to the PDI central core, and we present data that indicates a comparable optoelectronic dichotomy can be engineered by design into PDI peptide nanomaterials. This research highlights the power of synergistic feedback loops between computational and experimental peptide nanomaterial design in the context of realizing advanced optoelectronic function.

Methods

Experimental Methods

General Information

N-Methyl-2-pyrrolidone (NMP) was obtained from Advanced ChemTech. Pyridine was obtained from Alfa-Aesar. Dichloromethane (DCM) was freshly distilled prior to storage. All solvents were stored over 4 Å molecular sieves and were subsequently degassed by sparging with nitrogen gas 30 min prior to use. O-(Benzotriazol-1-yl)-N,N,N'N'-tetramethyluronium hexafluorophosphate (HBTU) was purchased from Oakwood Products Inc. Wang resin (preloaded with amino acid) and Fmoc-protected amino acids were obtained from Advanced Chem Tech. All other reagents and starting materials were obtained from Sigma-Aldrich and were used as received. General Solid-Phase Peptide Synthesis (SPPS). All peptides were synthesized using the standard Fmoc solid-phase technique with Wang resin preloaded with Fmoc-protected valine (Wang-Val, 0.700 mmol/g). To the resin in a peptide chamber, Fmoc-deprotection was accomplished by adding a 20% piperidine solution in DMF twice (successive 5 and 10 min treatments) followed by washing with NMP \times 3, methanol \times 3, and DCM \times 3. For the amino acid couplings, 3.0 equiv of the Fmocprotected amino acid was activated with 2.9 equiv of HBTU and 10 equiv of diisopropylethylamine (DIPEA) in NMP, and this solution was added to the resin beads. The reaction mixture was allowed to mix for 45-90 min, after which the beads were rinsed with NMP, methanol, and DCM (3 times each). The completion of all couplings was monitored using a Kaiser test on a few dry resin beads, repeating the same amino acid coupling as needed. The general procedure for amino acid coupling was repeated for each additional amino acid until the desired peptide sequence was obtained. Last amino acid was deprotected using piperidine solution leaving a -NH₂ terminated resin.

General On-Resin Dimerization Procedure. Following a previously reported literature,⁴³ -NH₂ terminated resin (0.10 mmol) and 3,4,9,10-Perylenetetracarboxylic dianhydride (PDA) (0.012 g, 0.031 mmol) were transferred to the Schlenk flask equipped with a reflux condenser. The mixture was dried under vacuum and was suspended in pyridine (5.0 mL) thereafter. This suspension was

heated to 65 °C followed by the addition of diisopropyl ethyl amine (0.25 mL, 1.5 mmol) and reaction was further heated to 135 °C for 10-12 hours. A second portion of PDA (0.008 g, 0.02 mmol) was added along with a second portion of pyridine (3.0 mL). Reaction was maintained at 135 °C and continued for an additional 10-12 hours. Resin was cooled to room temperature, filtered and washed with MeOH. The resin was then suspended in pyridine (6.0 mL), heated to 65 °C followed by the addition of diisopropyl ethyl amine (0.25 mL, 1.5 mmol) and further heated to 135 °C for 6 hours. Resin was cooled to room temperature.

General Peptide Cleavage and Workup Procedure. Following dimerization, the resin was returned to the peptide chamber and again subjected to a standard wash cycle: $1 \times H_2O$, 1×2 -Propanol, $1 \times CH_3CN$, $2 \times NMP$, $2 \times methanol$, and $2 \times DCM$. The resin was treated with 14.25 mL of trifluoroacetic acid, 375 μ L of water, and 375 μ L of triisopropylsilane for 2 h. The peptide solution was filtered from the resin beads, washed 3 times with DCM, and concentrated by evaporation under reduced pressure. The crude peptide was then precipitated from solution with 60–80 mL of diethyl ether and isolated through centrifugation. The resulting pellet was triturated with diethyl ether to yield crude product, which was dissolved in approximately 15–20 mL of water and 50 μ L of potassium hydroxide (1 M) and lyophilized.

Characterization details of peptide-pi molecules can be found in the supporting information.

Electrospray Ionization Mass Spectrometry (ESI-MS). ESI samples were collected using a Thermo Finnigan LCQ Deca Ion Trap Mass Spectrometer in negative mode. Samples were prepared in a 1:1 MeOH:water solution with 1% ammonium hydroxide.

Reverse-Phase HPLC. HPLC purification was performed on an Agilent 1100 series (semipreparative/analytical) and a Varian PrepStar SD-1 (preparative) instrument using Luna 5

µm particle diameter C8 with TMS end-capping columns with silica solid support. An ammonium formate aqueous buffer (pH 8) and acetonitrile were used as the mobile phase.

UV-vis and Photoluminescence. UV-vis spectra were obtained using a Varian Cary 50 Bio UV-vis spectrophotometer. Photoluminescence spectra were obtained using a PTi Photon Technology International Fluorometer (QuantaMaster 40) with a 75 W Ushio Xenon short arc lamp and operated with Felix32 Version 1.2 software. Spectroscopic samples were prepared by diluting the peptide solution to the appropriate concentration (concentration mentioned in spectra captions) in Millipore water. Neutral condition refers to the sample only in Millipore water at appropriate concentration. The pH was then adjusted by adding 15 μ L of 1M KOH for basic solutions and 40 μ L of 1M HCl for acidic solutions.

Circular Dichroism (CD). CD spectra were obtained using a Jasco J-810 spectropolarimeter. Spectroscopic samples were prepared by diluting the peptide solution to the appropriate concentration (concentration mentioned in spectra captions) in Millipore water. Neutral condition refers to the sample only in Millipore water at appropriate concentration. The pH was then adjusted by adding 25 μL of 1M KOH for basic solutions and 60 μL of 1M HCl for acidic solutions.

Dynamic Light Scattering (DLS). DLS spectra were obtained using a Zetasizer Nano-ZS90 (Malvern Instruments). Spectroscopic samples were prepared by diluting the peptide solution to the appropriate concentration (concentration mentioned in spectra captions) in Millipore water. Neutral condition refers to the sample only in Millipore water at appropriate concentration. The pH was then adjusted by adding 15 μ L of 1M KOH for basic solutions and 40 μ L of 1M HCl for acidic solutions.

Attenuated total reflection Fourier transform infrared (ATR-FTIR). ATR-FTIR spectra were obtained on lyophilized acidic peptide solutions using a Thermo Scientific Nicolet iD5 ATR-IR. Transmission Electron Microscopy (TEM). Imaging was performed on a FEI Technai 12 TWIN transmission electron microscope equipped with an SIS Megaview III CCD digital camera at an accelerating voltage of 100 kV. Acidic solutions (0.02 wt %) of each peptide were prepared by placing the samples in a closed container with a vial of conc. HCl opened within, which initiated the assembly process by diffusion of HCl vapor to the sample. The peptides were pipetted (drop

25 °C. Excess solution was wicked off by touching the side of the grid to filter paper. The samples were then stained with a 2% uranyl acetate solution, and excess moisture was wicked off. The grid was allowed to dry in air before imaging.

of 1 mg/mL solution) onto 200 mesh copper grids coated with carbon and incubated for 5 min at

Computational Methods

All-atom molecular modeling

All molecular dynamics simulations of the DAVG, DAIA, VEVAG, and VEVAA peptides were performed using GROMACS 2019.2 simulation suite⁴⁴ patched with the PLUMED v. 2.5.2⁴⁵ enhanced sampling libraries. Each π-conjugated peptide was modeled using the AMBER99SB-ILDN⁴⁶ forcefield with all-atom topologies generated using the AnteChamber PYthon Parser interfacE (ACPYPE)⁴⁷ wrapper for ANTECHAMBER (AmberTools17.0) (D.A. Case, D.S. Cerutti, T.E. Cheatham, III, T.A. Darden, R.E. Duke, T.J. Giese, H. Gohlke, A.W. Goetz, D.Greene,N. Homeyer, S. Izadi, A. Kovalenko, T.S. Lee, S. LeGrand, P. Li, C. Lin, J. Liu, T. Luchko, R. Luo,D. Mermelstein, K.M. Merz, G. Monard, H. Nguyen, I. Omelyan, A. Onufriev, F. Pan, R. Qi, D.R. Roe, A.Roitberg, C. Sagui, C.L. Simmerling, W.M. Botello-Smith, J. Swails, R.C.

Walker, J. Wang, R.M. Wolf, X.Wu, L. Xiao, D.M. York and P.A. Kollman (2017), AMBER 2017, University of California, San Francisco.). The ionizable Asp and Glu side chains and two C-termini carboxylates were prepared in a fully protonated state corresponding to low-pH (pH < 1) conditions. Partial charges were obtained using the Restrained Electrostatic Potential (RESP) method^{48, 49} with calculations performed in Gaussian 16⁵⁰ at the B3LYP/6-31G(d) level of theory. Water solvent was modeled using the TIP3P water model⁵¹. The leapfrog algorithm was used to numerically integrate forward Newton's equations of motion with a timestep of 2 fs. 52 Simulations were performed in three-dimensional cuboidal simulation boxes with periodic boundary conditions. The LINCS algorithm⁵³ was used to constrain all covalent bonds with hydrogen atoms. Lennard-Jones interactions were smoothly shifted to zero at a 1.0 nm cutoff and particle mesh Ewald (PME)⁵⁴ with a real space cutoff of 1.0 nm and a Fourier grid spacing of 0.16 nm were used to treat Coulombic interactions. The real space cutoff and Fourier grid spacing values are optimized during runtime for performance. A Parrinello-Rahman barostat⁵⁵ and velocity rescaling thermostat⁵⁶ were used to control pressure and temperature, respectively. Initial system configurations were subjected to steepest descent energy minimization to eliminate forces larger 10 kJ/mol.nm and initial velocities assigned by sampling from a Maxwell-Boltzmann distribution at 300 K. Systems were then equilibrated under 100 ps of simulation in the NVT ensemble at 300 K followed by 100 ps of simulation in the NPT ensemble at 300 K and 1 bar.

Well-tempered metadynamics calculations

The potential of mean force (PMF) as a function of the signed twist angle θ between a pair of oligopeptides within a molecular dimer were estimated using well-tempered metadynamics⁵⁷, following a protocol that we have previously reported^{21, 58}. In brief, we perform well-tempered

metadynamics along the single collective variable (CV) defined as the signed twist angle θ between the PDI cores of a dimerized pair of molecules:

$$\theta = \arccos(\mathbf{m}_1 \cdot \mathbf{m}_2) \cdot \operatorname{sgn}((\mathbf{m}_1 \times \mathbf{m}_2) \cdot \mathbf{d}). \tag{1}$$

Here, m_1 and m_2 are vectors that connect the terminal nitrogen atoms of the PDI core of arbitrarily labeled molecule 1 and molecule 2, respectively, and d is a vector that points from the center of mass (COM) of the PDI core of molecule 1 to molecule 2. The magnitude of the angle between the two PDI cores is captured in the first term $arccos(m_1 \cdot m_2)$ of eq 1 that is endowed with a positive or negative sign by the second term $sgn((\boldsymbol{m}_1 \times \boldsymbol{m}_2) \cdot \boldsymbol{d})$ that captures that handedness of the dimer configuration via the sign of the projection of d onto the cross product $m_1 \times m_2$. A positive signed twist angle (θ >0) corresponds to M-type (left-handed) chirality, while a negative signed twist angle (θ <0) corresponds to P-type (left-handed) chirality. Sampling is focused on the range $\theta \in [-1.25, 1.25]$ radians by applying a harmonic restraint with force constant $k_{\theta} = 1000$ kJ/mol.rad² if θ departs this range. To maintain the integrity of the dimer, an additional harmonic restraint with force constant $k_d = 1000 \text{ kJ/mol.nm}^2$ was applied to the COM distance | d| between the aromatic cores of the two molecules if $|\mathbf{d}| > 0.6$ nm for the smaller DAVG system and $|\mathbf{d}| > 0.6$ 0.7 nm for the larger DAIA, VEVAA, and VEVAG systems. Each dimer was initialized with |d|= 0.45 nm and θ = +10° and solvated within a 7×6×4 nm³ simulation box with TIP3P water.⁵¹ Periodic boundary conditions were implemented in all three dimensions. The box was designed to be sufficiently large to accommodate at least 1.50 nm of spacing between any atom in the dimer pair and box edges such that there are no spurious interactions between periodic images of the dimer.

Well-tempered metadynamics simulations were performed using the PLUMED enhanced sampling libraries⁴⁵ patched to GROMACS 2019.2⁴⁴. Calculations were performed independently for each system and trajectory snapshots saved every 10 ps for analysis. Each metadynamics production run used the signed twist angle θ as the biasing CV and deposited Gaussians with initial height of 1.2 kJ/mol and width 0.2 radians every 1 ps using a bias factor of γ = 20.0 for the DAVG, DAIA, and VEVAG systems, and γ = 22.5 for the VEVAA system. We define convergence by ensuring that both (1) the height of the Gaussians deposited by the well-tempered metadynamics falls to approximately zero (< ~0.05 kJ/mol) indicating that the bias potential has converged, and (2) collective sampling along the signed twist angle θ becomes approximately uniform, defined by the criterion that the fraction of configurations with θ <0 and θ >0 is within ~5%. Convergence was achieved in the DAVG and DAIA systems after 7 μ s of simulation, and in the VEVGA and VEVAA systems after 6 μ s and 5.61 μ s, respectively.

The well-tempered metadynamics potentials of mean force are used to estimate the cumulative probability distribution (CDF) in the absolute magnitude of the signed twist angle $CDF(|\theta|)$. This function measures the integrated probability of observing the system with a twist angle of magnitude $|\theta|$ or smaller. Given the unbiased probability density function $P(\theta)$, the probability of observing a dimer at or below a given twist angle magnitude is given by:

$$CDF(|\theta|) = \frac{\int_{-\theta}^{\theta} P(\theta^*) d\theta^*}{\int_{-\pi/2}^{\pi/2} P(\theta^*) d\theta^*} \approx \frac{\sum_{i=0}^{N} w_i \quad if \ |\theta_i| \le |\theta| \ and \ |d_i| \le d_{cut} \ else \ 0}{\sum_{i=0}^{N} w_i \quad if \ |\theta_i| \le 1.25 \ and \ |d_i| \le d_{cut} \ else \ 0'}$$
(2)

where the second expression represents the numerical estimate computed from our well-tempered metadynamics runs in which we approximate the integrals as sums. The index i iterates over the N simulation snapshots saved over the course of the metadynamics run, and w_i is the weight associated with each frame under reweighting to the unbiased ensemble. The summations are

restricted to the volume of phase space over which the angular and COM harmonic restraints are not active, corresponding to $|\theta_i| < 1.25$ and $|d_i| < d_{cut}$, where d_{cut} =0.6 nm for DAVG and d_{cut} =0.7 nm for DAIA, VEVAA, and VEVAG, to remain within our definition of a dimer pair defined during our metadynamics simulation. It is useful to observe that in the case of an unbiased simulation there would be no externally applied bias and each weight $w_i = \frac{1}{N}$ in the summation and eq 2 reduces to counting the fraction of configurations with $|\theta_i| < |\theta|$.

Umbrella sampling calculations

Umbrella sampling was performed in the COM distance |d| between a pair of peptides in order to estimate the dimerization potential of mean force curves quantifying the free energy change for the assembly of an equilibrium dimer. Calculations were performed using GROMACS 2019.2 and the data analyzed using the g wham module implementing the Weighted Histogram Analysis Method (WHAM)⁵⁹ and applying the entropic correction^{44,60}. Dimers were initialized at the signed twist angle θ corresponding to the global minimum of the free energy landscapes in θ computed by well-tempered metadynamics (see Well-tempered metadynamics calculations) and then subjected to energy minimization and relaxation (see All-atom molecular modeling). In all cases, the angle θ deviated no more than 15° from its initial value after performing the relaxation. The box dimensions were chosen to be 7.5×7.5×7.5 nm³ for the VEVAG and VEVAA molecules and 12×12×12 nm³ for the DAVG and DAIA molecules. In each case the box was sufficiently large that there were no spurious interactions between periodic images of the molecules through the periodic boundaries even at the largest values of |d| considered. A steered molecular dynamics simulation was then performed to pull the dimerized pair apart to a distance of |d| = 3.5 nm by applying a force constant of 1000 kJ/mol.nm² to the COM distance |d|. Frames extracted from this pulling trajectory were used to initialize umbrella sampling calculations at particular values of |d|.

We stratified sampling into 16 umbrella sampling windows at a spacing of 0.2 nm over the range $|\mathbf{d}| = 0.3$ -3.3 nm. Each umbrella simulation was performed in the NPT ensemble at 300 K and 1 bar and was first equilibrated for 100 ps before being subjected to a 10 ns production run. Harmonic umbrella potentials were applied with spring constants $k_u = 1000 \text{ kJ/mol.nm}^2$ and centered on the initial value of $|\mathbf{d}|$ within the window. As necessary, additional umbrella windows were run to fill in any gaps in the overlap between the umbrella window histograms and the PMF is recalculated with g_wham . Uncertainties are estimated by performing three independent sets of umbrella sampling simulations for each system.

Results and Discussion

Validation of the computational guidance. We prepared the two sequences revealed from computational screening to have high co-facial PDI stacking, corresponding to a high degree of geometric overlap of the PDI π -cores rather than an optimal geometry that would favor electrical transport or exciton migration. The sequence space screened in this initial assessment was constrained to four amino acid residues within the peptide flanking wings, with the terminal position fixed as aspartic acid (D) in order to impart pH sensitivity to the assembly process. The peptides are effectively ionized and dissolved at basic pH, although there is computational and experimental evidence of molecular pre-association/aggregation (see Figures S23-25). The assembly into tape/fibril-like nanomaterials is initiated upon protonation of the terminal carboxylates at acidic pH. In these determined sequences, it is notable that both DAIA and DAVG have a relatively small residue closest to the PDI core (A or G) and a larger hydrophobic group in the next position (I or V). Using standard Fmoc-based solid-phase peptide synthesis in conjunction with our past methods to incorporate the PDI π -system (see experimental section/SI), PDI cores were substituted with the DAIA and DAVG sequences (Figure 1). Our experimental and

computational investigation revealed the two distinct types of self-assembled architectures from these PDI-peptide conjugates.

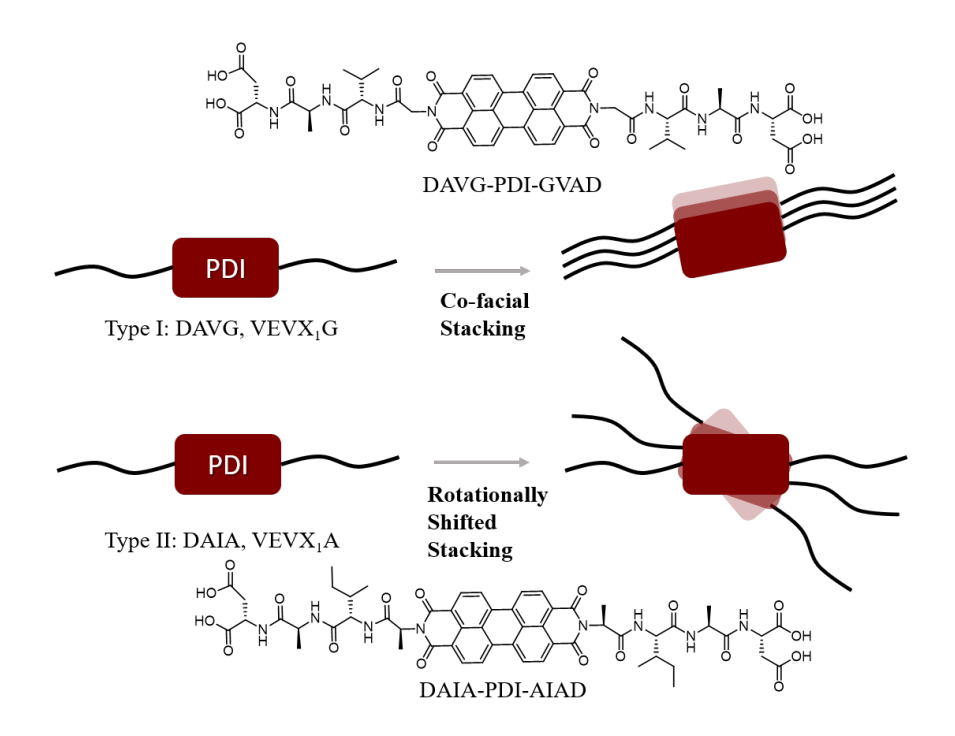


Figure 1. Chemical structures of the DAVG-PDI-GVAD and DAIA-PDI-AIAD peptides inspired by computational input.

These peptides form 1-D tape-like nanostructures when exposed to acidic aqueous environments in line with other related molecules (**Figure 2**), and the photophysical responses were probed in basic (*ca.* pH ~12.5), neutral (*ca.* pH ~7), and acidic (*ca.* pH ~1.2) media to observe the extent of self-association at different pH. The UV-Vis responses of DAVG-PDI under basic and neutral conditions showed signatures typical of PDI chromophores: two distinct peaks at 535 nm and 502 nm corresponding to 0-0 and 0-1 transitions, respectively. The ratio of 0-0/0-1 peak is about 0.61 and 0.70 in basic and neutral medium similar to the ratio observed for other PDI-conjugated materials in aqueous medium.^{62, 63} These band ratio values are in between the ratio expected for PDI-monomer (>1.4) and stacked dimers or aggregates (<0.6).^{62, 64} However, acidic environments resulted in a broad absorption profile with new peaks arising around 450 nm, 585

nm and 625 nm (Figure 2). A distinct color change from red to black was also observed upon going from basic to acidic media. Previously, these types of shifts in absorption maxima were explained by formation of liquid crystalline-type materials, ^{38, 65, 66} J-aggregates ^{67, 68} or mixture of H- and J-aggregates⁴⁰. However, similar broadening and characteristic shifts of absorption maxima have also been reported in perylene monoimide systems due to charge transfer and Frenkel state mixing. 69-71 This mixing allows for extended exciton separation and an elongated charge transfer band. DAIA showed a similar response to DAVG in the neutral medium, but the clear separation between 0-0 and 0-1 peaks was not as pronounced in the basic medium. The ratio of 0-0/0-1 peak is about 0.89 and 0.86 respectively for basic and neutral medium, which is higher than the ratio observed for DAVG indicating presence of more monomeric structure. 63, 64 The spectral response of DAIA under acidic conditions was vastly different from DAVG, maintaining the general signature observed under basic conditions for both DAVG and DAIA, which is the prototypical UV-Vis signature of PDI chromophores. This relatively broader and unstructured absorption spectrum with reduced extinction coefficient is hallmark of H-type assembled structure in PDIconjugated molecules in aqueous solution. ^{64, 69} We classify these two different photophysical responses within the acidic aggregates as Type-I (DAVG-PDI) and Type-II (DAIA-PDI) for the rest of the article.

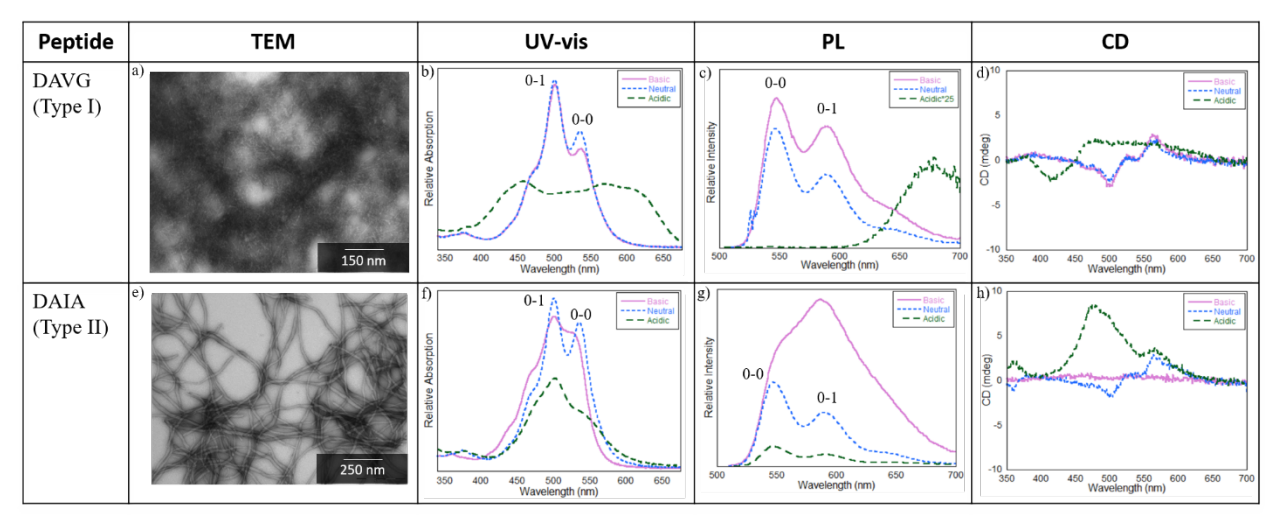


Figure 2. Transmission electron microscopy (TEM) images of assembled peptides (a, e), UV-Vis (b, f), PL (c, g) and CD (d,h) spectroscopy traces of DAVG (a-d) and DAIA (e-h) peptides in basic (solid pink), neutral (blue short dash), and acidic (green long dash) media. UV-Vis and PL spectra were recorded at 5-7.5 μ M concentration range. CD spectra were recorded at 15-20 μ M concentration range.

PL spectroscopy of DAVG-PDI in neutral and basic media showed three distinct peaks around 540 nm, 590 nm and 640 nm. The peak around 640 nm was previously assigned to H-aggregate formation whereas the 540 nm and 590 nm peaks can be assigned to the 0-0 and 0-1 transitions, respectively.⁶⁸ The basic medium showed higher fluorescence intensity as compared to neutral solution due to the greater degree of molecular dissolution. The acidic solution of DAVG formed a broad low-energy excimer like signal (λ_{max} ~ 675 nm) which was observed previously in liquid-crystalline or J-aggregate materials.⁶⁵⁻⁶⁸ DAIA showed a similar response to DAVG in neutral media. However, in basic media, the 0-1 transition, which had lower intensity in neutral condition as compared to the 0-0 transition, showed a prominent rise, and the peak around 640 nm was not observed which may be buried in the red-tail of the 0-1 peak. It is possible that a subtle change in aggregation occurred in basic media which was also evident from the slightly different spectral shapes apparent in the UV-Vis spectra. However, the higher intensity of signal in basic medium can again be attributed to the disassembly of aggregates. The acidic assembled DAIA

sample showed high-energy 'exciton' like vibronic signatures similar to the neutral and basic solutions, in stark contrast to assembled DAVG.

CD spectroscopy of DAVG-PDI showed weak Cotton effects in basic and neutral media around 0-0 and 0-1 transition similar to other PDI-oligopeptide assemblies, indicating weak exciton-coupled states. Acidic media presented different signatures: low-energy absorption bands which suggested that the molecules were in a chiral environment, and a weakly bisignate higher-energy 450 nm band which indicated weak exciton coupling. At basic pH, DAIA showed no characteristic signal indicating no interaction between the chromophores. However, it showed a weak Cotton effect in neutral solution as observed by a crossover at the wavelength coinciding with the absorption maxima. This shows similarity to DAVG in neutral medium indicating that pisystems are weakly exciton-coupled in neutral media forming similar types of assemblies. Further lowering the pH showed no crossover around the absorption maxima, however the intensity of signal was increased indicating the molecules are held in a chiral environment.

Expansion and generalization of the mined sequences. The molecular simulations of Thurston and Ferguson predicted high alignment propensities for both DAVG-PDI and DAIA-PDI, but the observed photophysical profiles reported herein showed vastly different responses. We hypothesized that residues closer to the π -core may have significant influence on the assembly process and the resulting photophysical response. Thus, we extended our investigation to a related series of peptide-PDI conjugates inspired by the initial computational guidance based on the general VEVX₁X₂ sequence tagged to the PDI core (**Figure 3**). This peptide was chosen based on our prior work that showed the VEVAG pentapeptide to be a good consensus sequence to form peptide- π -peptide conjugates when appended to a variety of chromophores, all of which displayed good aqueous solubility at basic pH and 1-D assembly fidelity at acidic pH. We varied the steric

bulk of the side-chains of amino acids at the X_1 position using glycine (G, R = H), alanine (A, R = CH₃), valine (V, R = CH(CH₃)₂) and phenylalanine (F, R = CH₂Ph). Attempts to vary the steric bulk at the X_2 position were met with some difficulties due to the proximity to the PDI core: we could only achieve the addition of glycine (G, R = H) and alanine (A, R = CH₃). We found previously that more hydrophobic residues formed closely coupled aggregate states due to the higher van der Waals-type interaction among residues outcompeting aqueous solvation. However, these more hydrophobic residues can also lead to the increased steric crowding within these assemblies. These systematic variations of 'steric bulk' at different positions of the pentapeptide sequence provide some guidance about the effect of amino acids on internal structure and optoelectronic properties of the PDI-based assemblies.

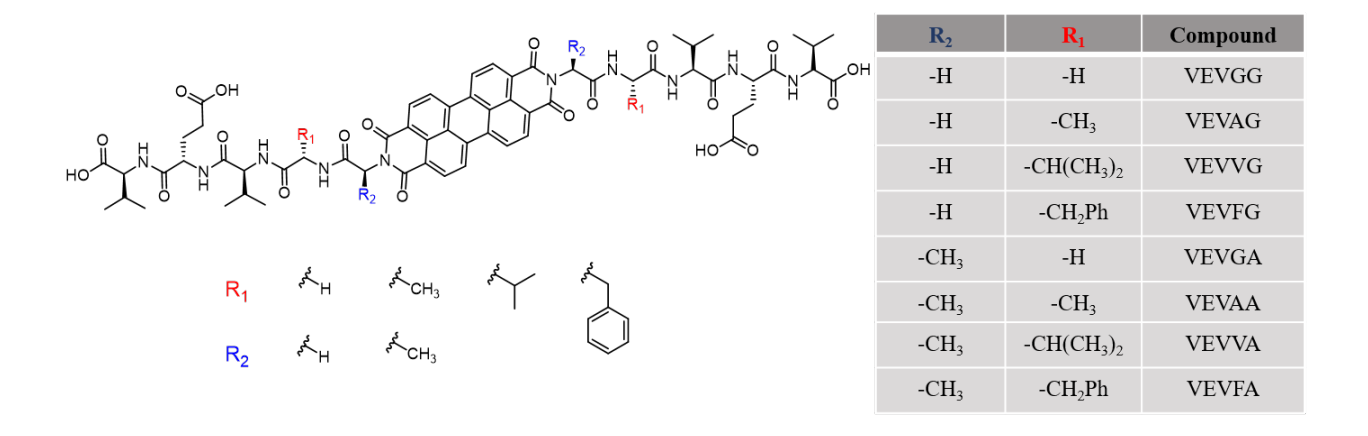


Figure 3. Chemical structures of the members of the VEVX₁X₂-PDI-X₂X₁VEV peptide libraries.

1-D tapelike nanostructures with high aspect ratios were visualized from all of the VEVX₁X₂ peptides when aqueous basic solutions (0.2 mg/mL) were exposed to HCl vapor within a closed chamber. In general, the nanostructures were micrometers in length and comparable to other peptide- π -peptide conjugates reported previously. The switching of amino acids in the X₁ and X₂ positions did not have any significant impact on the overall one-dimensionality of the supramolecular nanostructures; however, the width of the nanostructures varied significantly. For

example, VEVAG presented widths of 8.8 ± 0.9 nm while VEVAA had widths of 14.5 ± 0.7 nm. These two peptides are shown as representative examples of nanostructures in **Figure 4**.

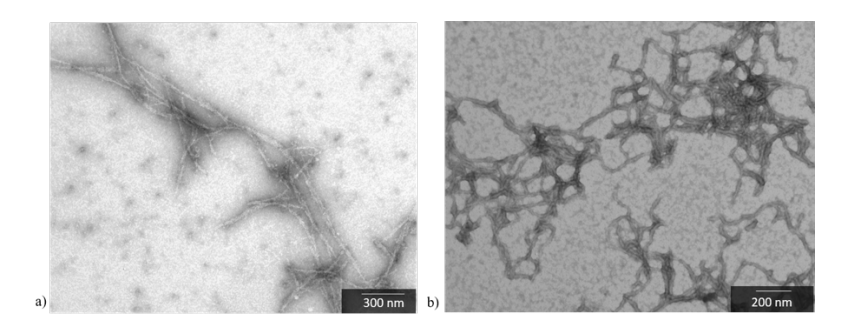


Figure 4. TEM images of a) VEVAG, and b) VEVAA from acidic solution of concentration 0.2 mg/mL.

VEVX₁G peptides recorded similar photophysical responses to that of DAVG (Type I). UV-Vis spectroscopy showed two distinct peaks at 535 and 502 nm under basic and neutral media (representative example in Figure 5a). However, the absorption recorded from acidic solution showed broadening for all the peptides similar to the Type-I response but with slight variation in intensity and magnitude. VEVGG showed absorption maxima around 480 nm and 560 nm and the broadening was lesser than the other peptides of this family. VEVAG and VEVVG showed absorption maxima around 450 nm and relatively broader signals. VEVFG showed a maximum around 465 nm and additional peaks were observed at 530 nm and 560 nm (Figure 5b). The photophysical responses from VEVX₁A peptides matched that from DAIA (Type II). The representative absorption profile of VEVAA is shown in Figure 5c. Generally, two peaks (i.e. 535 nm corresponding to 0-0 transition and 502 nm corresponding to 0-1 transition) were observed for this family of peptides regardless of the condition, but the intensity varied significantly. In basic media, the 0-0/0-1 peak intensity ratio increased indicative of aggregate dissolution. Acidic solutions showed higher weight towards the 0-1 peak indicating H-type assembly processes for all the peptides in this family.

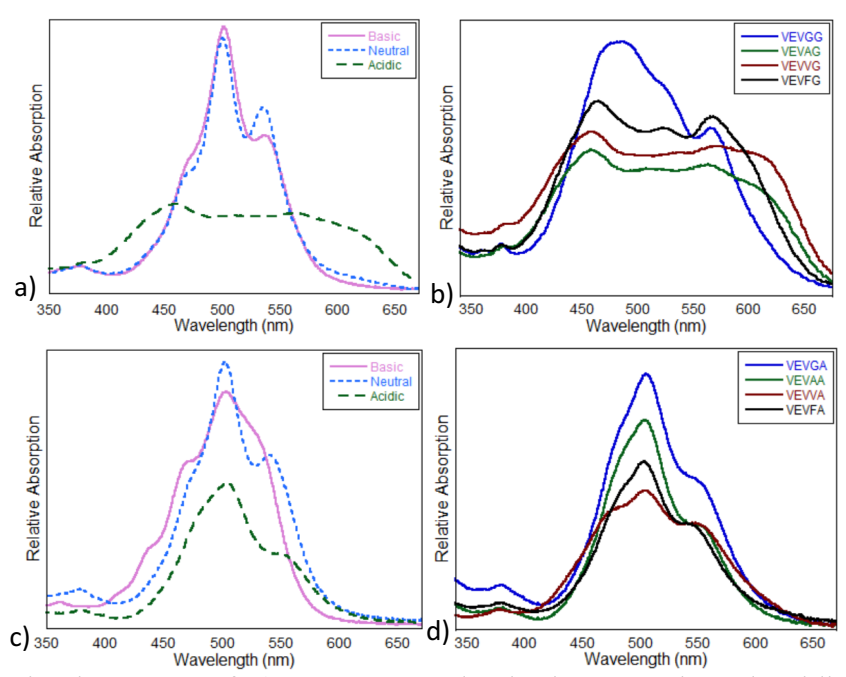


Figure 5. UV-Vis signatures of a) VEVAG under basic, neutral, and acidic conditions, b) VEVX₁G peptides under acidic conditions, c) VEVAA under basic, neutral, and acidic conditions, and d) VEVX₁A peptides under acidic conditions. All the spectra were recorded at 5-7.5 μ M concentration range.

Generally, all VEVX₁G peptides showed similar PL signals to that of Type I DAVG-PDI. Emissive responses with clear vibronic structures were observed under basic and neutral conditions whereas acidic solutions showed broad emissive signals. (VEVAG as a representative example is shown in **Figure 6a**). VEVAG showed more of a quenched signal at basic pH as compared to the neutral medium which is indicative of salt-driven assembly process at higher pH. Similarly, VEVX₁A peptides showed similar emission responses to Type II DAIA-PDI as anticipated by the UV-vis responses. Upon lowering the pH, signal quenching was observed but the peak positions remained unchanged, which is typical of weakly-coupled H-type aggregates. VEVAA PL is shown as a representative example in **Figure 6b**. Here, a new excimer peak started to arise (around 675 nm) reminiscent of what was observed for Type-I peptides, but the other features mirror those of the Type II DAIA peptides. This low energy excimeric peak was absent for VEVGA but more pronounced for VEVVA and VEVFA. These data indicate the distinctive

nature of variation of steric bulk with respect to particular position in the peptidic backbone of peptide-PDI conjugates.

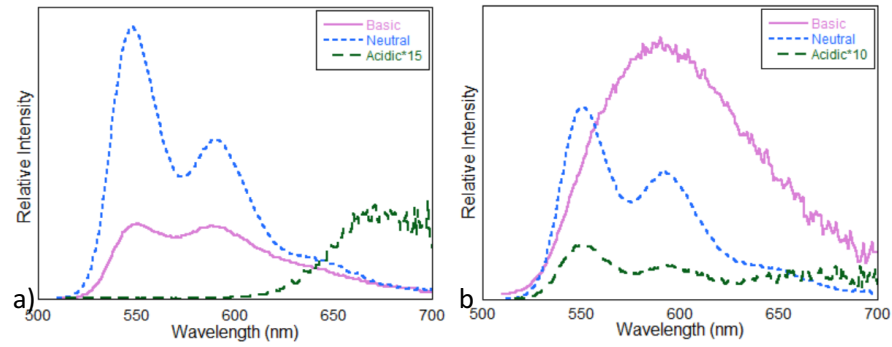


Figure 6. PL signature of a) VEVAG under basic, neutral, and acidic condition. b) VEVAA under basic, neutral, and acidic condition. All the spectra were recorded at 5-7.5 μM concentration range.

VEVX₁G peptides show relatively weak Cotton effects under basic and neutral conditions, reminiscent of the DAVG Type I peptide. CD spectroscopy revealed uniform profiles under acidic media for all the peptides: low-energy absorption bands suggesting that the molecules are in chiral environments, and high-energy bands (e.g. 450-480 nm) that were exciton coupled as observed via signal crossover at an absorption maxima (for a representative example, see **Figure 7a**). VEVGG showed a relatively stronger Cotton effect in acidic medium which is expected as it also shows different signature in UV-Vis spectroscopy from the other peptides in the same family. VEVX₁A peptides recorded similar signatures to the Type-II DAIA peptide. Peptides in basic media showed no CD signature indicating a lack of interaction between chromophores or other local chirality. Upon lowering the pH to neutrality, Cotton effects were observed for the low-energy band i.e. around 500 nm. The high-energy CD features indicated that the chromophores are in chiral environment but not specifically exciton coupled. Further lowering the pH to acidic, the intensity of Cotton effect increased indicating strong exciton coupling in between chromophores (see **Figure 7b** for a representative example).

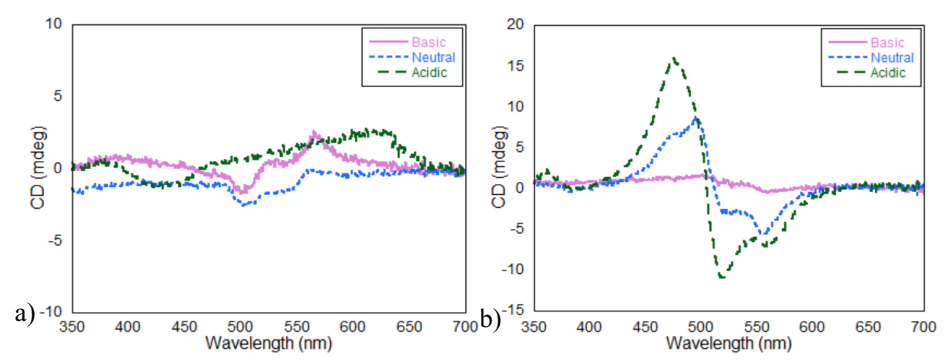


Figure 7. CD signature of a) VEVAG under basic, neutral, and acidic condition. b) VEVAA under basic, neutral, and acidic condition. All the spectra were recorded at 15-20 μ M concentration range.

Molecular modeling of pi-peptide packing and stability. To gain insight into the molecular structure and dynamics of the self-assembled aggregates, we performed all-atom molecular dynamics simulations of the DAVG, DAIA, VEVAG, and VEVAA systems under acidic conditions where experimental assembly into self-assembled nanoaggregates was observed. We adopt a reductionist posture in which we study the behavior of a dimer pair as representative of the behavior of molecules with larger multibody aggregates. In doing so we sacrifice explicit representation of multibody effects for a minimal system whose thermally accessible configurational phase space we can exhaustively sample using enhanced simulation techniques to obtain converged estimates of dimer structure and stability (see *Computational Methods*). We have previously adopted this approach to gain molecular-level understanding of the determinants of supramolecular chirality and demonstrated good agreement between the computational prediction and experimental measurements using circular dichroism.^{21,58}

We report in **Figure 8** the potential of mean force (PMF) as a function of signed twist angle θ between the two members of the molecular dimer for each of the DAVG, DAIA, VEVAG, and VEVAA peptide systems. The signed twist angle θ is defined as the relative angle subtended between the two PDI cores and is defined mathematically in **eq. 1**. A signed twist angle of θ =0 corresponds to cofacial parallel stacking, a positive signed twist angle (θ >0) to M-type (left-

handed) chirality, and a negative signed twist angle (θ <0) to P-type (left-handed) chirality. The PMFs for each of the four systems exhibit two-well character, with local free energy minima in the θ >0 (M-type, left-handed) and θ <0 (P-type, right-handed) portions of the range. The relative depths of these free energy minima expose the relative preferences for left- versus right-handed packing of the dimer. Our results identify very little preference in chirality for DAVG and VEVAG, with the free energy difference between the two wells lying at or below the 1 kT level of thermal fluctuations – where k is Boltzmann's constant and T is the absolute temperature – with $\Delta\beta F = (0.14 \pm 0.04)$ kT and $\Delta\beta F = (0.98 \pm 0.14)$ kT for DAVG and VEVAG, respectively. Conversely, our calculations do predict a weak thermodynamic preference for left-handed (M-type) supramolecular chirality for DAIA ($\Delta\beta F = (3.5 \pm 0.4)$ kT) and VEVAA ($\Delta\beta F = (1.5 \pm 0.3)$ kT). These results suggest that a (left-handed) chiral preference is associated with the placement of a bulkier Ala residue in the X₂ position adjacent to the PDI core.

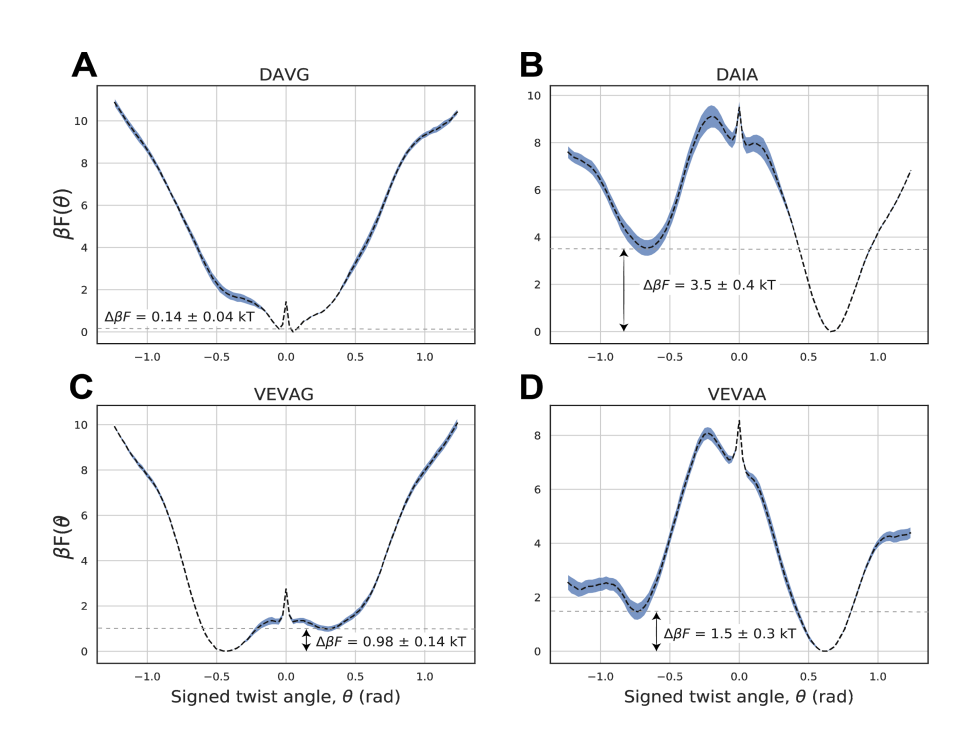


Figure 8. Potential of mean force (PMF) as a function of signed twist angle (θ) recovered from well-tempered metadynamics simulations of (A) DAVG, (B) DAIA, (C) VEVAG, and (D)

VEVAA. Metadynamics simulations consider a dimerized pair of molecules biased along the collective variable defined as the signed twist angle (θ). Annotations indicate the difference in free energy $\Delta\beta F$ between the local free energy minima in the θ >0 and θ <0 regimes. Standard errors are illustrated by shading and were estimated by block averaging our trajectories into five equally sized contiguous blocks.

To further explore this observation, we report in **Figure 9** the cumulative distribution functions in the absolute magnitude of the signed twist angle $CDF(|\theta|)$ for each of the four systems. This quantity reports the equilibrium probability of observing a dimer with a twist angle of magnitude $|\theta|$ or less. In comparing DAVG vs. DAIA and VEVAG vs. VEVAA, we observe that the presence of a smaller Gly residue in the X_2 position immediately adjacent to the PDI core results in a higher prevalence of smaller magnitude twist angles compared to the presence of a bulkier Ala residue that leads to an elevated preference for larger magnitude twist angles.

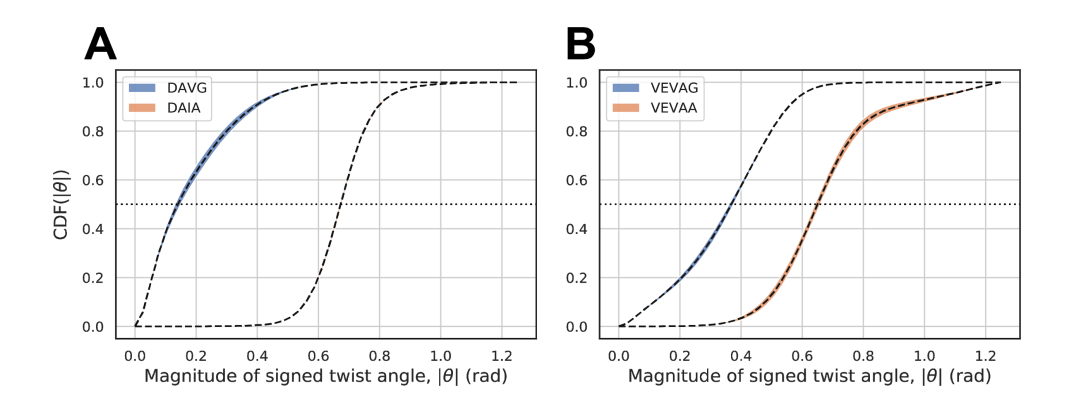


Figure 9. Cumulative distribution function (CDF) for the probability of observing a dimer pair at or below a given signed twist angle magnitude $|\theta|$ for (A) DAVG vs. DAIA and (B) VEVAG vs. VEVAA. Shading represents standard errors estimated by block averaging where each trajectory is split into five equally sized contiguous blocks. The placement of the smaller Gly residue in the X_2 position immediately adjacent to the PDI core leads to a higher observed probability of smaller magnitude twist angles, whereas its replacement with a bulkier Ala residue leads to a higher prevalence of larger magnitude twist angles.

To assess the thermodynamic driving force for self-assembly, we report in **Figure 10** the dimerization potential of mean force curves for the four systems. In all cases we observe dimerization to be spontaneous, with a free energetic driving force for dimerization of approximately $\Delta\beta F \approx 25\text{-}35$ kT. This favorable driving force is consistent with experimental

observations of spontaneous self-assembly under low-pH conditions. Comparing DAVG vs. DAIA and VEVAG vs. VEVAA, we observe that the peptides possessing a Gly residue in the X_2 position immediately adjacent to the PDI core possess a $\Delta\Delta\beta F\approx 5$ -10 kT more favorable dimerization free energy compared to those with a bulkier Ala residue in this position.

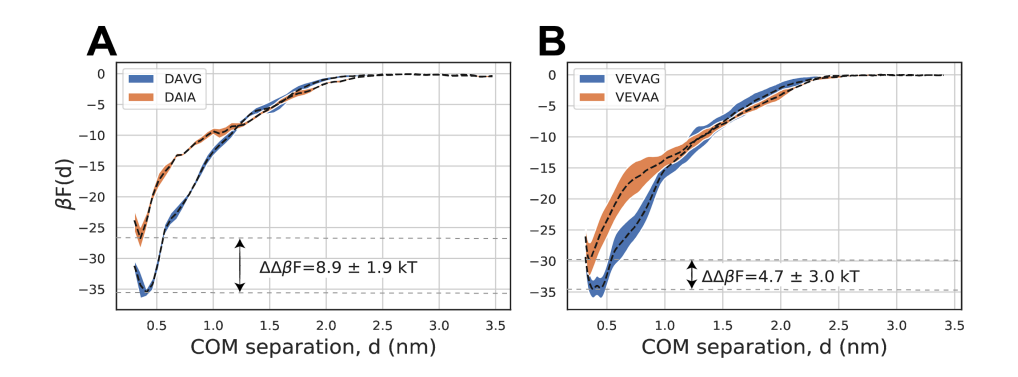


Figure 10. Potential of mean force (PMF) as a function of dimer aromatic core COM separation for (A) DAVG and DAIA, and (B) VEVAG and VEVAA extracted from umbrella sampling simulations. Shading represents pointwise standard errors estimated from three independently run sets of umbrella sampling simulations for each system. The arbitrary zero of free energy is defined for the non-interacting system at large COM separation, |d|. Annotations indicate the difference in the dimerization free energies between the two peptide systems $\Delta\Delta\beta F$. The presence of a proximate Gly residue in the X₂ position immediately adjacent to the PDI core results in a more favorable free energy of dimerization than the presence of an Ala residue in the same position.

Taken together, the higher prevalence of smaller twist angles and more favorable dimerization free energy for the DAVG/VEVAG systems compared to DAIA/VEVAA suggest that the systems possessing the smaller Gly residue in the X_2 position produce aggregates that are more cofacially aligned and more strongly bound than those possessing the bulkier Ala residue in the X_2 position that are more twisted and less strongly associated. These results are consistent with experimental UV-Vis and PL spectra wherein the DAVG/VEVAG systems exhibited Type I (i.e., J-aggregate and/or liquid-crystalline) photophysical behavior upon acidification, whereas DAIA/VEVAA exhibited Type II (i.e., weakly coupled H-aggregate) behavior (Table 1, Fig. 4,5). These calculations provide a molecular-level rationale for the two different classes of observed behavior as a function of the steric bulk of the amino acid residue in the X_2 position: bulkier

residues induce weaker association and reduced cofacial packing. **Figure 1** summarizes the influence of amino acid residues to the formation of self-assembled architecture of PDI-peptide conjugates.

Conclusion

We designed a series of peptide-PDI-peptide materials that shows a broad range of absorption and emission properties as effected by small changes in the composition of the amino acid sequence. This is the first example of systematic tuning of hydrophobicity and size in polypeptide-conjugated PDI molecules to attain distinct photophysical responses in aqueous solution. We established that lower hydrophobicity/size of the amino acids (i.e. glycine) closest to the PDI core drives the formation of Type-I structures which can be J-aggregates or liquid-crystalline type materials or a mixture of both. Small changes in hydrophobicity from a side chain of –H to –CH₃ results in Type-II structures which can be interpreted as weakly coupled H-type aggregates. All-atom molecular dynamics simulations provide molecular-level corroboration that this small change in the hydrophobic side-chain of the core-adjacent amino acid residue can substantially alter the aggregated structures by modulating the relative orientation between chromophores and the binding strength between neighboring peptides within the supramolecular aggregate. This study provides new insight about how different electronic couplings between PDI chromophores can be controllably engineered by modest changes in the amino acid sequence and provides a platform to exploit and study previously inaccessible PDI electronic states in aqueous solution. Using initial computational insight followed by tandem experimental and computational analysis, we identified a general structure/function relationship between amino acid sequences and photophysical properties in PDI-polypeptide conjugates that can be used in future to design new aqueous selfassembled electronic materials.

Supporting Information. Synthesis procedures, ESI mass spectrometry data, HPLC data, TEM images, DLS data, FT-IR spectra, UV-vis spectra, PL spectra and CD spectra.

Acknowledgements

This research is based upon work supported by the National Science Foundation's Designing Materials to Revolutionize and Engineer our Future (DMREF) program (Grant Nos. DMR-1728947 and DMR-1841807). K.S. is supported by the National Science Foundation's Graduate Research Fellowship (Grant No. DGE-1746045). This work was completed in part with resources provided by the University of Chicago Research Computing Center. We gratefully acknowledge computing time on the University of Chicago high-performance GPU-based cyberinfrastructure (Grant No. DMR-1828629).

Conflict of Interest Statement

A.L.F. is a co-founder and consultant of Evozyne, LLC and a co-author of US Provisional Patents 62/853,919 and 62/900,420 and International Patent Applications PCT/US2020/035206 and PCT/US20/50466.

References

- 1. Hoeben, F. J. M.; Jonkheijm, P.; Meijer, E. W.; Schenning, A. P. H. J. About Supramolecular Assemblies of π-Conjugated Systems. *Chem. Rev.* **2005**, *105* (4), 1491–1546.
- 2. Hasegawa, M.; Iyoda, M. Conducting Supramolecular Nanofibersand Nanorods. *Chem. Soc. Rev.* **2010**, *39*, 2420–2427.
- 3. Aida, T.; Meijer, E. W.; Stupp, S. I. Functional Supramolecular Polymers. *Science* **2012**, *335* (6070), 813–817.
- 4. Moulin, E.; Cid, J. J.; Giuseppone, N. Advances in Supramolecular Electronics From Randomly Self-Assembled Nanostructures to Addressable Self-Organized Interconnects. *Adv. Mater.* **2013**, *25*, 477–487.

- 5. Schenning, A. P. H. J.; Jonkheijm, P.; Peeters, E.; Meijer, E. W. Hierarchical Order in Supramolecular Assemblies of Hydrogen-Bonded Oligo(*p*-phenylene vinylene)s. J. Am. Chem. Soc. **2001**, *123*, 409-416.
- 6. Panda, S. S.; Katz, H. E.; Tovar, J. D. Solid-State Electrical Applications of Protein and Peptide Based Nanomaterials. *Chem. Soc. Rev.* **2018**, *47*, 3640–3658.
- 7. Marty, R.; Nigon, R.; Leite, D.; Frauenrath, H. Two-Fold Odd-Even Effect in Self-Assembled Nanowires from Oligopeptide-Polymer-Substituted Perylene Bisimides. *J. Am. Chem. Soc.* **2014**, *136* (10), 3919–3927.
- 8. Chworos, A.; Severcan, I.; Koyfman, A. Y.; Weinkam, P.; Oroudjev, E.; Hansma, H. G.; Jaeger, L. Building Programmable Jigsaw Puzzles with RNA. *Science* **2004**, *306*, 2068–2072.
- 9. Lovley, D. R. Electrically Conductive Pili: Biological Function and Potential Applications in Electronics. *Curr. Opin. Electrochem.* **2017**, *4*, 190–198.
- 10. Amit, M.; Yuran, S.; Gazit, E.; Reches, M.; Ashkenasy, N. Tailor-Made Functional Peptide Self-Assembling Nanostructures. *Adv. Mater.* **2018**, *30*, 1707083.
- 11. Tovar, J. D. Supramolecular Construction of Optoelectronic Biomaterials. *Acc. Chem. Res.* **2013**, *46* (7), 1527–1537.
- 12. Kumar, M.; Ing, N. L.; Narang, V.; Wijerathne, N.; Hochbaum, A. I.; Ulijn, R. V. Amino Acid-Encoded Biocatalytic Self-Assembly Enables the Formation of Transient Conducting Nanostructures. *Nat. Chem.* **2018**, *10*, 696–703.
- 13. Shao, H.; Seifert, J.; Romano, N. C.; Gao, M.; Helmus, J. J.; Jaroniec, C. P.; Modarelli, D. A.; Parquette, J. R. Amphiphilic Self-Assembly of an n-Type Nanotube. *Angew. Chem. Int. Ed.* **2010**, *49*, 7688 –7691.
- 14. Tsai, W.-W.; Tevis, I. D.; Tayi, A. S.; Cui, H.; Stupp, S. I. Semiconducting Nanowires from Hairpin-Shaped Self-Assembling Sexithiophenes. *J. Phys. Chem. B* **2010**, *114*, 14778–14786.
- 15. Khalily, M. A.; Bakan, G.; Kucukoz, B.; Topal, A. E.; Karatay, A.; Yaglioglu, H. G.; Dana, A.; Guler, M. O. Fabrication of Supramolecular n/p-Nanowires via Coassembly of Oppositely Charged Peptide-Chromophore Systems in Aqueous Media. *ACS Nano* **2017**, *11*, 6881–6892.
- 16. Kumar, R. J.; MacDonald, J. M.; Singh, T. B.; Waddington, L. J.; Holmes, A. B. Hierarchical Self-Assembly of Semiconductor Functionalized Peptide Alpha-Helices and Optoelectronic Properties. *J. Am. Chem. Soc.* **2011**, *133*, 8564–8573.
- 17. Lee, T.; Panda, S. S.; Tovar, J. D.; Katz, H. E. Unusually Conductive Organic-Inorganic Hybrid Nanostructures Derived from Bio-Inspired Mineralization of Peptide/Pi-Electron Assemblies. *ACS Nano* **2020**, *14*, 1846-1855.
- 18. Cornil, J.; dos Santos, D. A.; Crispin, X.; Silbey, R.; Brédas, J. L. Influence of interchain interactions on the absorption and luminescence of conjugated oligomers and polymers: a quantum chemical characterization. *J. Am. Chem. Soc.* **1998**, *120*, 1289–1299.
- 19. Siddiqui, S.; Spano, F. C. H- and J-aggregates of conjugated polymers and oligomers: a theoretical investigation. *Chem. Phys. Lett.* **1999**, *308*, 99–105.
- 20. Wall, B. D.; Zacca, A. E.; Sanders, A. M.; Wilson, W. L.; Ferguson, A. L.; Tovar, J. D. Supramolecular Polymorphism: Tunable Electronic Interactions within π-Conjugated Peptide Nanostructures Dictated by Primary Amino Acid Sequence. *Langmuir* **2014**, 30 (20), 5946–5956.

- 21. Panda, S. S.; Shmilovich, K.; Ferguson, A. L.; Tovar, J. D. Computationally Guided Tuning of Amino Acid Configuration Influences the Chiroptical Properties of Supramolecular Peptide-π-Peptide Nanostructures. *Langmuir* **2020**, *36*, 6782-6792.
- 22. Wang, M.; Zhou, P.; Wang, J.; Zhao, Y.; Ma, H.; Lu, J. R.; Xu, H. Left or Right: How Does Amino Acid Chirality Affect the Handedness of Nanostructures Self-Assembled from Short Amphiphilic Peptides? *J. Am. Chem. Soc.* **2017**, *139* (11), 4185–4194.
- 23. Lin, S.; Li, Y.; Li, B.; Yang, Y. Control of the Handedness of Self-Assemblies of Dipeptides by the Chirality of Phenylalanine and Steric Hindrance of Phenylalycine. *Langmuir* **2016**, *32* (29), 7420-7426.
- 24. Pashuck, T.; Cui, H. Stupp, S. I. Tuning Supramolecular Rigidity of Peptide Fibers through Molecular Structure. *J. Am. Chem. Soc.* **2010**, *132*, 6041–6046.
- 25. Würthner, F.; Stolte, M. Naphthalene and perylene diimides for organic transistors. *Chem. Commun.*, **2011**, *47*, 5109–5115.
- 26. Greenfield, S. R.; Svec, W. A.; Gosztola, D.; Wasielewski, M. R. Multistep Photochemical Charge Separation in Rod-like Molecules Based on Aromatic Imides and Diimides. *J. Am. Chem. Soc.*, **1996**, *118*, 6767–6777.
- 27. Draper, E. R.; Greeves, B. J.; Barrow, M.; Schweins, R.; Zwijnenburg, M. A.; Adams, D. J. pH-Directed Aggregation to Control Photoconductivity in Self-Assembled Perylene Bisimide Films. *Chem*, **2017**, *2*, 716–731.
- 28. Huang, C.; Barlow, S.; Marder, S. R. Perylene-3,4,9,10-tetracarboxylic Acid Diimides: Synthesis, Physical Properties, and Use in Organic Electronics. *J. Org. Chem.*, **2011**, *76*, 2386–2407.
- 29. Horowitz, G. K., F.; Spearman, P.; Fichou, D.; Nogues, C.; Pan, X.; Garnier, F. Evidence for n-type conduction in a perylene tetracarboxylic diimide derivative. *Adv. Mater.* **1996**, *8*, 242–244.
- 30. Rajaram, S.; Armstrong, P. B.; Kim, B. J.; Frechet, J. M. J. Effect of Addition of a Diblock Copolymer on Blend Morphology and Performance of Poly(3-hexylthiophene):Perylene Diimide Solar Cells. *Chem. Mater.* **2009**, *21*, 1775–1777.
- 31. Dayneko, S. V.; Rahmati, M.; Pahlevani, M.; Welch, G. C. Solution processed red organic light-emitting-diodes using an N-annulated perylene diimide fluorophore. *J Mat. Chem. C* **2020**, *8*, 2314-2319.
- 32. Klebe, G.; Graser, F.; Hadicke, E.; Berndt, J. Crystallochromy as a solid-state effect: correlation of molecular conformation, crystal packing and colour in perylene-3,4:9,10-bis(dicarboximide) pigments. *Acta Crystallogr.* **1989**, *B45*, 69–77.
- 33. Roy, S.; Maiti, D. K.; Panigrahi, S.; Basak, D.; Banerjee, A. A new hydrogel from an amino acid-based perylene bisimide and its semiconducting, photo-switching behaviour *RSC Advances*, **2012**, *2*, 11053–11060.
- 34. Draper, E. R.; Walsh, J. J.; McDonald, T. O.; Zwijnenburg, M. A.; Cameron, P. J.; Cowan, A. J.; Adams, D. J. Air-stable Photoconductive Films Formed from Perylene Bisimide Gelators. *J. Mater. Chem. C* **2014**, *2*, 5570–5575.
- 35. Draper, E. R.; Archibald, L. J.; Nolan, M. C.; Schweins, R.; Zwijnenburg, M. A.; Sproules, S.; Adams, D. J. Controlling Photoconductivity in PBI Films by Supramolecular Assembly. *Chem. Eur. J.* **2018**, *24*, 4006 4010.

- 36. Datar, A.; Balakrishnan, K.; Zang, L. One-dimensional self-assembly of a water soluble perylene diimide molecule by pH triggered hydrogelation *Chem. Commun.*, **2013**, *49*, 6894–6896.
- 37. Gallaher, J. K.; Aitken, E. J.; Keyzers, R. A.; Hodgkiss, J. M. Controlled aggregation of peptide-substituted perylene-bisimides. *Chem. Commun.*, **2012**, *48*, 7961–7963.
- 38. Eakins, G. L.; Gallaher, J. K.; Keyzers, R. A.; Falber, A.; Webb, J. E. A.; Laos, A.; Tidhar, Y.; Weissman, H.; Rybtchinski, B.; Thordarson, P.; Hodgkiss, J. M. Thermodynamic Factors Impacting the Peptide-Driven Self-Assembly of Perylene Diimide Nanofibers. *J. Phys. Chem. B* **2014**, *118*, 8642–8651.
- 39. Eakins, G. L.; Pandey, R.; Wojciechowski, J. P.; Zheng, H. Y.; Webb, J. E. A.; Valery, C; Thordarson, P.; Plank, N. O. V.; Gerrard, J. A.; Hodgkiss, J. M. Functional Organic Semiconductors Assembled via Natural Aggregating Peptides. *Adv. Funct. Mater.*, **2015**, *25*, 5640–5649.
- 40. Marty, R.; Szilluweit, R.; Sánchez-Ferrer, A.; Bolisetty, S.; Adamcik, J.; Mezzenga, R.; Spitzner, E-C; Feifer, M.; Steinmann, S. N.; Corminboeuf, C.; Frauenrath, H. Hierarchically Structured Microfibers of "Single Stack" Perylene Bisimide and Quaterthiophene Nanowires. *ACS Nano* **2013**, *7*, 10, 8498–8508.
- 41. Bai, S.; Debnath, S.; Javid, N.; Frederix, P. W. J. M.; Fleming, S.; Pappas, C.; Ulijn, R. V. Differential Self-Assembly and Tunable Emission of Aromatic Peptide Bola-Amphiphiles Containing Perylene Bisimide in Polar Solvents Including Water. *Langmuir* **2014**, *30*, 7576–7584.
- 42. Thurston, B. A.; Ferguson, A. L. Machine learning and molecular design of self-assembling conjugated oligopeptides. *Mol. Simul.* **2018**, *44*, 930–945.
- 43. Vadehra, G. S.; Wall, B. D.; Diegelmann, S. D.; Tovar, J. D. On-resin Dimerization Incorporates a Diverse Array of π-conjugated Functionality Within Aqueous Self-assembling Peptide Backbones. *Chem. Comm.* **2010**, *46*, 3947-3949.
- 44. Abraham, M. J.; Murtola, T.; Schulz, R.; Smith, J. C.; Hess, B.; Lindahl, E. GROMACS: High Performance Molecular Simulations through Multi-Level Parallelism from Laptops to Supercomputers. *SoftwareX* **2015**, *1-2*, 19–25.
- 45. Tribello, G. A.; Bonomi, M.; Branduardi, D.; Camilloni, C.; Bussi, G. PLUMED 2: New Feathers for an Old Bird. *Comput. Phys. Commun.* **2014**, *185* (2), 604–613.
- 46. Lindorff-Larsen, K.; Piana, S.; Palmo, K.; Maragakis, P.; Klepeis, J. L.; Dror, R. O.; Shaw, D. E. *Proteins* **2010**, *78*, 1950–1958.
- 47. Sousa da Silva, A.W., Vranken, W.F. ACPYPE AnteChamber PYthon Parser interfacE. BMC Res Notes **2012**, *5*, 367.
- 48. Reynolds, C. A.; Essex, J. W.; Richards, W. G. Atomic Charges for Variable Molecular Conformations. *J. Am. Chem. Soc.* **1992**, *114*, 9075–9079.
- 49. Bayly, C. I.; Cieplak, P.; Cornell, W.; Kollman, P. A. A Well-behaved Electrostatic Potential Based Method Using Charge Restraints for Deriving Atomic Charges: the RESP Model. *J. Phys. Chem.* **1993**, *97*, 10269–10280.
- 50. Gaussian 16, Revision C.01, M. J. Frisch, G. W. Trucks, H. B. Schlegel, G. E. Scuseria, M. A. Robb, J. R. Cheeseman, G. Scalmani, V. Barone, G. A. Petersson, H. Nakatsuji, X. Li, M. Caricato, A. V. Marenich, J. Bloino, B. G. Janesko, R. Gomperts, B. Mennucci, H. P.

- Hratchian, J. V. Ortiz, A. F. Izmaylov, J. L. Sonnenberg, D. Williams-Young, F. Ding, F. Lipparini, F. Egidi, J. Goings, B. Peng, A. Petrone, T. Henderson, D. Ranasinghe, V. G. Zakrzewski, J. Gao, N. Rega, G. Zheng, W. Liang, M. Hada, M. Ehara, K. Toyota, R. Fukuda, J. Hasegawa, M. Ishida, T. Nakajima, Y. Honda, O. Kitao, H. Nakai, T. Vreven, K. Throssell, J. A. Montgomery, Jr., J. E. Peralta, F. Ogliaro, M. J. Bearpark, J. J. Heyd, E. N. Brothers, K. N. Kudin, V. N. Staroverov, T. A. Keith, R. Kobayashi, J. Normand, K. Raghavachari, A. P. Rendell, J. C. Burant, S. S. Iyengar, J. Tomasi, M. Cossi, J. M. Millam, M. Klene, C. Adamo, R. Cammi, J. W. Ochterski, R. L. Martin, K. Morokuma, O. Farkas, J. B. Foresman, and D. J. Fox, Gaussian, Inc., Wallingford CT, 2016.
- 51. Mark, P.; Nilsson, L. Structure and Dynamics of the TIP3P, SPC, and SPC/E Water Models at 298 K. *J. Phys. Chem. A* **2001**, *105*, 9954–9960.
- 52. Hockney, R. W. Computer Simulation Using Particles; CRC Press: Boca Raton, 1988.
- 53. Hess, B.; Bekker, H.; Berendsen, H. J. C.; Fraaije, J. G. E. M. LINCS: A Linear Constraint Solver for Molecular Simulations. *J. Comput. Chem.* **1997**, *18* (12), 1463–1472.
- 54. Essmann, U.; Perera, L.; Berkowitz, M. L. A smooth particle mesh Ewald method. *J. Chem. Phys.* **1995**, *103*, 8577–8593.
- 55. Parrinello, M.; Rahman, A. Polymorphic Transitions in Single Crystals: A New Molecular Dynamics Method. *J. Appl. Phys.* **1981**, *52*, 7182–7190.
- 56. Bussi, G.; Donadio, D.; Parrinello, M. Canonical Sampling through Velocity Rescaling. *J. Chem. Phys.* **2007**, *126*, 014101.
- 57. Barducci, A.; Bussi, G.; Parrinello, M. Well-Tempered Metadynamics: A Smoothly Converging and Tunable Free-Energy Method. *Phys. Rev. Lett.* **2008**, *100*, 020603.
- 58. Panda, S. S.; Shmilovich, K.; Ferguson, A. L.; Tovar, J. D. Controlling Supramolecular Chirality in Peptide-π-Peptide Networks by Variation of the Alkyl Spacer Length. Langmuir 2019, 35, 14060–14073.
- 59. Hub, J. S.; Groot, B. L.; Spoel, D. g_wham—A Free Weighted Histogram Analysis Implementation Including Robust Error and Autocorrelation Estimates. *J. Chem. Theory Comput.* **2010**, *6*, 3713–3720.
- 60. Pall, S.; Abraham, M. J.; Kutzner, C.; Hess, B.; Lindahl, E. Tackling Exascale Software Challenges in Molecular Dynamics Simulations with GROMACS. In: Markidis S., Laure E. (eds) Solving Software Challenges for Exascale. EASC 2014. Lecture Notes in Computer Science, 2015, 8759. Springer, Cham.
- 61. Valverde, L. R.; Thurston, B. A.; Ferguson, A. L.; Wilson, W. L. Evidence for Prenucleated Fibrilogenesis of Acid-Mediated Self-Assembling Oligopeptides via Molecular Simulation and Fluorescence Correlation Spectroscopy. *Langmuir*, **2018**, *34*, 7346-7354.
- 62. Mishra, A. K.; Weissman, H.; Krieg, E.; Votaw, K. A.; McCullagh, M.; Rybtchinski, B.; Lewis, F. D. Self-Assembly of Perylenediimide–Single-Strand-DNA Conjugates: Employing Hydrophobic Interactions and DNA Base-Pairing to Create a Diverse Structural Space. *Chem Eur. J.* **2017**, *23*, 10328 10337.
- 63. Ashcraft, A.; Liu, K.; Mukhopadhyay, A.; Paulino, V.; Liu, C.; Bernard, B.; Husainy, D.; Phan, T.; Olivier, J.-H. A Molecular Strategy to Lock-in the Conformation of a Perylene Bisimide-Derived Supramolecular Polymer. *Angew. Chem., Int. Ed.* **2020**, *59*, 7487–7493.

- 64. Gorl, D.; Zhang, X.; Wurthner, F. Molecular Assemblies of Perylene Bisimide Dyes in Water. *Angew. Chem. Int. Ed.* **2012**, *51*, 6328-6348.
- 65. Cormier, R. A.; Gregg, B. A. Synthesis and Characterization of Liquid Crystalline Perylene Diimides. *Chem. Mater.* **1998**, *10*, 1309-1319.
- 66. Xu, Y.; Leng, S.; Xue, C.; Sun, R.; Pan, J.; Ford, J.; Jin, S. A Room-Temperature Liquid-Crystalline Phase with Crystalline π Stacks. *Angew. Chem. Int. Ed.* **2007**, *46*, 3896 –3899.
- 67. Wu, H.; Xue, L.; Shi, Y.; Chen, Y.; Li, X. Organogels Based on J- and H-Type Aggregates of Amphiphilic Perylenetetracarboxylic Diimides. Langmuir **2011**, *27*, 3074–3082.
- 68. Wagner, W.; Wehner, M.; Stepanenko, V.; Ogi, S.; Würthner, F. Living Supramolecular Polymerization of a Perylene Bisimide Dye into Fluorescent J-Aggregates *Angew. Chemie Int Ed*, **2017**, *129*, 16224–16228.
- 69. Hestand, N. J.; Spano, F. C. Expanded Theory of H- and J-Molecular Aggregates: The Effects of Vibronic Coupling and Intermolecular Charge Transfer. *Chem. Rev.* **2018**, *118*, 7069-7163.
- 70. Hestand, N. J.; Kazantsev, R. V.; Weingarten, A. S.; Palmer, L. C.; Stupp, S. I.; Spano, F. C. Extended-Charge-Transfer Excitons in Crystalline Supramolecular Photocatalytic Scaffolds *J. Am. Chem. Soc.*, **2016**, *138*, 11762–11774.
- 71. Oleson, A.; Zhu, T.; Dunn, I. S.; Bialas, D.; Bai, Y.; Zhang, W.; Dai, M.; Reichman, D. R.; Temeplaar, R.; Huang, L.; Spano, F. C. Perylene Diimide-Based Hj- and hJ-Aggregates: The Prospect of Exciton Band Shape Engineering in Organic Materials. *J Phys Chem C* **2019**, *123*, 20567-20578.

Table of Content Image

